China Ocean Eng., 2023, Vol. 37, No. 1, P. 53–61
DOI: https://doi.org/10.1007/s13344-023-0005-7, ISSN 0890-5487
http://www.chinaoceanengin.cn/ E-mail: coe@nhri.cn

System Identification and Parameter Self-Tuning Controller on Deep-Sea Mining Vehicle

WENG Qi-wang[a, b, c], YANG Jian-min[a, b, c, *], LIANG Qiong-wen[a, b, c], MAO Jing-hang[a, b, c], GUO Xiao-xian[a, b, c]

[a] SJTU Yazhou Bay Institute of Deepsea SCI-TECH, Sanya 572000, China

[b] State Key Laboratory of Ocean Engineering, Shanghai Jiao Tong University, Shanghai 200240, China

[c] Institute of Marine Equipment, Shanghai Jiao Tong University, Shanghai 200240, China

Received February 21, 2022; revised October 20, 2022; accepted December 7, 2022

Abstract

System identification is a quintessential measure for real-time analysis on kinematic characteristics for deep-sea mining vehicle, and thus to enhance the control performance and testing efficiency. In this study, the system identification algorithm, recursive least square method with instrumental variables (IV-RLS), is tailored to model 'Pioneer I', a deep-sea mining vehicle which recently completed a 1305-meter-deep sea trial in the Xisha area of the South China Sea in August, 2021. The algorithm operates on the sensor data collected from the trial to obtain the vehicle's kinematic model and accordingly design the parameter self-tuning controller. The performances demonstrate the accuracy of the model, and prove its generalization capability. With this model, the optimal controller has been designed, the control parameters have been self-tuned, and the response time and robustness of the system have been optimized, which validates the high efficiency on digital modelling for precision control of deep-sea mining vehicles.

Key words: deep-sea mining, system identification, parameter self-tuning controller, digital modeling

Citation: Weng, Q.W., Yang, J.M., Liang, Q.W., Mao, J.H., Guo, X.X., 2023. System identification and parameter self-tuning controller on deep-sea mining vehicle. China Ocean Eng., 37(1): 53–61, doi: https://doi.org/10.1007/s13344-023-0005-7

1 Introduction

Deep-sea mining technology is widely accepted as an efficient solution to resource depletion problem, in which the heavy-duty mining vehicle has become a hot research topic because of its high security, reliability, and strong ability to adapt to complex terrain (Zhou et al., 2013). However, massive size and component complexity of the deep-sea mining vehicle add up to the difficulty to launch and recovery in field work. The cost of sea trial is exorbitant, and the mechanical structure faces regular seawater corrosion, which brings many difficulties to research and testing of deep-sea mining vehicle. Digital modeling, in which system identification is considered as one of the most effective methods, plays a crucial role in operation monitoring and post-analysis in 3D structure design, multi-body dynamics analysis, health management and digital twin areas (Bai et al., 2018).

Digital modeling is usually divided into mechanism-based modeling and data-based modeling. In terms of mechanism-based modeling for tracked miner, Watanabe et al. (1993) established a kinematics model based on multi-rigid body dynamics theory, which could fit various terrains, including soft clay terrain. They also established a tracked-soil model to accurately reflect the inelastic response of soil under track pressure. While for the hinge link of the vehicle, Zhou et al. (2009) used ADAMS software to carry out the kinematic optimization design and dynamic analysis, and designed its solid model. For a variety of relative motions such as steering, pitching and rolling, ANSYS was adapted to check the strength of each component to verify the rationality of the design. Huang and Li (2019) focused on its speed control and trajectory tracking problem based on fuzzy control algorithm with LabVIEW.

However, it is hard to determine the performance parameters of heavy-duty vehicles, such as stiffness, damping and motion inertia. The elastic modulus, viscosity of hydraulic oil and damping ratio of the system also change with oil pressure, oil temperature and valve opening (Gao, 2006). Therefore, as for the kinematic characteristics of the vehicle, it is difficult to establish a suitable mathematical

Foundation item: The research was financially supported by the Hainan Provincial Joint Project of Sanya Yazhou Bay Science and Technology City (Grant No. 2021JJLH0078), the Science and Technology Commission of Shanghai Municipality (Grant No. 19DZ1207300) and the Major Projects of Strategic Emerging Industries in Shanghai.

*Corresponding author. E-mail: jmyang@sjtu.edu.cn

simulation model for actual scene without thorough consideration of the difference between the land and sea, mechanical corrosion, pressure deformation and water disturbance flow. Therefore, how to build a digital prototype with generalization ability based on sea trial data has become a research hotspot.

System identification is a generalized method based on data modeling, which determines the mathematical model to describe the system behavior according to the input and output, mainly for grey box problems. Most of the identification problems in engineering are incomplete identification problems, so that the crux of identification is order identification and the parameter estimation problems (Ji et al., 2008). Aiming at nonlinear servo system, myriad algorithms are proposed, including impulse response method (Yazid and Ng, 2021), high order frequency response method (Jia et al., 2020), correlation analysis method (Zamani and Badri, 2015), least square method (Li et al., 2018), maximum likelihood method (Wada et al., 2016) and random approximation algorithm (Kong et al., 2020). Takagi and Sugeno (Guan and Chen, 2004) proposed a nonlinear system identification method named T−S fuzzy model. The experimental results showed that this method converged quickly, but its fuzzy structure and rules were difficult to establish. Besides, it required a lot of manual intervention and was difficult for adaptive learning. Wang et al. (2020) proposed the algorithm 'nu'-support vector regression for the robust model establishment of ship maneuvering motion in nonparametric identification field. Zhang et al. (2008) proposed a neural network identification method based on genetic algorithm optimization, which solved the local minimum and perfect initial value requirement problems. The algorithm had high accuracy and fast convergence speed, but did not consider the influence of colored noise. A Radical Basis Function (RBF) neural network was adopted to identify the nonlinearity and time-varying parameters of dynamic pressure cylinder electrohydraulic servo system, improving the position tracking accuracy of the manipulator (Deng et al., 2018).

Least square method is one of the most widely used methods for system identification. For systems with white noise and high signal-to-noise ratio, this method can realize the uniform unbiased estimation. In order to apply the least square identification to the occasions where the actual noise characteristics are complex, many scholars have conducted indepth researches and proposed the augmented least square identification method (Guo et al., 2017), the deviation compensation least square identification method (Li and Shu, 2009), the generalized least square identification method (Deng and Ding, 2014) and the instrumental variable identification method (Chen et al., 2013). Among them, the recursive least square method is an iterative calculation method proposed for high dimensional matrices with long identification cycle, which intensely fits the multi-sensors system. It decomposes the parameterized model to identify the multivariable system and the complex coupling system on hierarchical principle and interactive estimation theory (Chen, 2009). As for data preprocess, the instrumental variable method can eliminate the estimation deviation caused by colored noise. The instrumental variables that are strongly correlated with the input and output data but not correlated with the system noise are selected so as to conduct unbiased estimation of the model parameters.

In this paper, a system identification method is proposed to model the deep-sea mining vehicle 'Pioneer I'. The contributions of this work are presented as follows:

(1) Providing a data-analysis method to obtain the kinematics characteristics, the transfer function and the controller design of deep-sea mining vehicle based on trial data.

(2) Proposing an IV-RLS algorithm (recursive least square method with instrumental variables) to solve the singular matrix problem and to eliminate the colored noise.

(3) Deducing a cyclic solution method to construct instrumental variables.

(4) Designing a parameter self-tuning controller with satisfactory control performance.

This paper is organized into five parts. The first part is a basic introduction to deep-sea mining vehicles and the research status, especially in the modeling and identification field. The second part is the unbiased estimation identification system primarily based on least square regression approach with instrumental variables, while a circular solution to instrumental variables selection is proposed. The third part is the brief case of 'Pioneer I', inclusive of electronic control system, hydraulic transmission device and analysis on the sea trial data in August 2021. The fourth part is the model simulation with statistic validation analysis, parameter self-tuning controller design and results comparison. The results exhibit that the model has high accuracy and generalization ability, and can be used for parameter self-tuning controller design, and can robotically optimize the response speed and robustness of the control system. The main conclusions are drawn in Section 5.

2 IV-RLS algorithm

This part is the analysis on the record data to be processed, the mathematic deduction of the algorithm and statistical characteristics. A circular solution method for instrumental variables selection is also proposed. Recursive least square algorithm minimizes the generalized error to identify the model. The instrumental variable method can eliminate the estimation deviation attributable to colored noise, as instrumental variables are strongly correlated with the input and output data but not correlated with the system noise. By IV-RLS algorithm, unbiased estimation of the model parameters is conducted.

2.1 Recursive least square estimation

In general, a control system can be expressed as:

$$y(k) = -a_1 y(k-1) - a_2 y(k-2) - \cdots - a_m y(k-m) + b_1 u(k-1) + b_2 u(k-2) + \cdots + b_n u(k-n) + d(k). \quad (1)$$

Among them, $y(k)$ is the system output while $u(k)$ is system input and $d(k)$ is the interference noise. $a_1, a_2, \cdots a_m$ and $b_1, b_2, \cdots b_n$ are the coefficients of the difference equation while n and m are respectively the numbers of zeros and poles of the system.

Further arranged into matrix form, the equations can be obtained:

$$y(k) = x^{\mathrm{T}}(k)\boldsymbol{\theta} + d(k); \quad (2)$$

$$\begin{cases} \boldsymbol{Y}(N) = [\ y(1)\ \ y(2)\ \ \cdots\ \ y(N)\ ]^{\mathrm{T}} \\ \boldsymbol{D}(N) = [\ d(1)\ \ d(2)\ \ \cdots\ \ d(N)\ ]^{\mathrm{T}} \\ \boldsymbol{X}(N) = \begin{bmatrix} \boldsymbol{x}(1) \\ \vdots \\ \boldsymbol{x}(k) \\ \vdots \\ \boldsymbol{x}(N) \end{bmatrix} = \begin{bmatrix} -y(0) & \cdots & -y(1-m) & u(0) & \cdots & u(1-n) \\ & \ddots & & & \ddots & \\ -y(k) & \cdots & -y(k-m) & u(k-1) & \cdots & u(k-n) \\ & \ddots & & & \ddots & \\ -y(N-1) & \cdots & -y(N-m) & u(N-1) & \cdots & u(N-n) \end{bmatrix} \end{cases} \quad (5)$$

Note: $\boldsymbol{X}(N)$ is only obtained at least after recording m groups of data. For concise representation, N=1 stands for the first time to calculate, namely $t = (1-m)$ is the initial time of the record.

2.2 Instrumental variables and cycle solution

For the parameter matrix to be estimated, the estimated objective function is:

$$J(\boldsymbol{\theta}) = \sum_{k=1}^{N} \left[y(k) - \boldsymbol{x}^{\mathrm{T}}(k)\boldsymbol{\theta} \right]^2 = [\boldsymbol{Y}(N) - \boldsymbol{X}(N)\boldsymbol{\theta}]^{\mathrm{T}} [\boldsymbol{Y}(N) - \boldsymbol{X}(N)\boldsymbol{\theta}]. \quad (6)$$

If the minimum value of $J(\boldsymbol{\theta})$ is taken, it should satisfy:

$$\frac{\partial J(\boldsymbol{\theta})}{\partial \boldsymbol{\theta}} = 0. \quad (7)$$

Derivative equations can be obtained:

$$\hat{\boldsymbol{\theta}} = \left[\boldsymbol{X}^{\mathrm{T}}(N)\boldsymbol{X}(N) \right]^{-1} \boldsymbol{X}^{\mathrm{T}}(N)\boldsymbol{Y}(N). \quad (8)$$

The conventional least square method takes all the data into the matrix to calculate the parameters directly. However, when the matrix dimension is large, it may be singular. The matrix inversion requires non-empty matrix. Thus, the recursive approach is used to solve it.

Here $\hat{\boldsymbol{\theta}}(k)$ stands for the parameter matric identified by the first k group data. With the estimate parameter $\hat{\boldsymbol{\theta}}(k)$ and observation data $y(k+1)$ and $u(k+1)$, the estimate parameter $\hat{\boldsymbol{\theta}}(k+1)$ can be obtained. The recursive principle is as follows:

Taking $\boldsymbol{P}(k) = \left[\boldsymbol{X}^{\mathrm{T}}(k)\boldsymbol{X}(k) \right]^{-1}$, it can be:

$$\boldsymbol{P}(k+1) = \left[\boldsymbol{P}^{-1}(k) + \boldsymbol{x}(k+1)\boldsymbol{x}^{\mathrm{T}}(k+1) \right]^{-1}. \quad (9)$$

Matrix inversion formula $(\boldsymbol{A} + \boldsymbol{BCD})^{-1} = \boldsymbol{A}^{-1} - \boldsymbol{A}^{-1}\boldsymbol{B}(\boldsymbol{C}^{-1} + \boldsymbol{DA}^{-1}\boldsymbol{B})^{-1}\boldsymbol{DA}^{-1}$ is also introduced:

$$\begin{cases} \boldsymbol{x}(k) = [-y(k-1)\ \ \cdots\ \ -y(k-m)\ \ u(k-1)\ \ \cdots\ \ u(k-n)]^{\mathrm{T}} \\ \boldsymbol{\theta} = [a_1\ \ \cdots\ \ a_m\ \ b_1\ \ \cdots\ \ b_n]^{\mathrm{T}} \end{cases} \quad (3)$$

where $\boldsymbol{\theta}$ is the parameter matrix to be identified.

There is $m+n$ unknown variables in Eq. (3) and $m > n$, so at least $2m$ equations are needed to solute the coefficients.

Taking $k = 1, 2, \cdots, N$, a linear equation group can be obtained, which is expressed as matrix form:

$$\boldsymbol{Y}(N) = \boldsymbol{X}(N)\boldsymbol{\theta} + \boldsymbol{D}(N); \quad (4)$$

$$\boldsymbol{P}(k+1) = \left[\boldsymbol{I} - \frac{\boldsymbol{P}(k)\boldsymbol{x}(k+1)\boldsymbol{x}^{\mathrm{T}}(k+1)}{1 + \boldsymbol{x}^{\mathrm{T}}(k+1)\boldsymbol{P}(k)\boldsymbol{x}(k+1)} \right] \boldsymbol{P}(k). \quad (10)$$

At this time, the parameter estimation $\hat{\boldsymbol{\theta}}(k+1)$ is:

$$\hat{\boldsymbol{\theta}}(k+1) = \hat{\boldsymbol{\theta}}(k) + \boldsymbol{P}(k+1)\boldsymbol{x}(k+1)\left[y(k+1) - \boldsymbol{x}^{\mathrm{T}}(k+1)\hat{\boldsymbol{\theta}}(k) \right]. \quad (11)$$

Taking $\boldsymbol{K}(k+1) = \boldsymbol{P}(k+1)\boldsymbol{x}(k+1)$, Eq. (11) is simplified as:

$$\hat{\boldsymbol{\theta}}(k+1) = \hat{\boldsymbol{\theta}}(k) + \boldsymbol{K}(k+1)\left[y(k+1) - \boldsymbol{x}^{\mathrm{T}}(k+1)\hat{\boldsymbol{\theta}}(k) \right]. \quad (12)$$

In summary, the recursive process is:

(1) Taking the observation data of the former k group, the initial estimation value $\hat{\boldsymbol{\theta}}(k)$ and update matrix $\boldsymbol{P}(k)$ are calculated.

(2) According to Eq. (10), the updated matrixs $\boldsymbol{P}(k+1)$ and $\boldsymbol{K}(k+1)$ are calculated, and the next estimation matrix $\hat{\boldsymbol{\theta}}(k+1)$ is finally obtained.

(3) The error at this time is calculated according to the objective function Eq. (6) at each recursion. If it is smaller than the expected threshold, it is terminated and $\boldsymbol{\theta}$ is identified.

2.3 Statistical characteristics analysis

Regression statistical characteristics analysis and unbiased estimation can be written as:

$$\hat{\boldsymbol{\theta}} = [\boldsymbol{X}^{\mathrm{T}}(N)\boldsymbol{X}(N)]^{-1}\boldsymbol{X}^{\mathrm{T}}(N)[\boldsymbol{X}(N)\boldsymbol{\theta} + \boldsymbol{D}(N)] = \boldsymbol{\theta} + [\boldsymbol{X}^{\mathrm{T}}(N)\boldsymbol{X}(N)]^{-1}\boldsymbol{X}^{\mathrm{T}}(N)\boldsymbol{D}(N). \quad (13)$$

The Mathematical expectation can be calculated:

$$E(\hat{\boldsymbol{\theta}}) = \boldsymbol{\theta} + [\boldsymbol{X}(N)^{\mathrm{T}}\boldsymbol{X}(N)]^{-1} E[\boldsymbol{X}(N)^{\mathrm{T}}\boldsymbol{D}(N)]. \quad (14)$$

It is easy to find that when the input signal is correlated with noise, it is a biased estimation.

Considering the complexity of dynamic noise, it is challenging to model it. In this paper, the method of constructing

instrumental variables is adopted, and the cyclic solution method is proposed.

The instrumental variable $\boldsymbol{H}$ is constructed:

$$\boldsymbol{H}^{\mathrm{T}}\boldsymbol{Y}(N)=\boldsymbol{H}^{\mathrm{T}}\boldsymbol{X}(N)\boldsymbol{\theta}+\boldsymbol{H}^{\mathrm{T}}\boldsymbol{D}(N) \tag{15}$$

and the estimation is:

$$\hat{\boldsymbol{\theta}}=\left[\boldsymbol{X}^{\mathrm{T}}(N)\boldsymbol{H}\boldsymbol{H}^{\mathrm{T}}\boldsymbol{X}(N)\right]^{-1}\left[\boldsymbol{H}^{\mathrm{T}}\boldsymbol{X}(N)\right]^{\mathrm{T}}\boldsymbol{H}^{\mathrm{T}}\left[\boldsymbol{X}(N)\boldsymbol{\theta}+\boldsymbol{D}(N)\right]=$$
$$\boldsymbol{\theta}+\left[\boldsymbol{X}^{\mathrm{T}}(N)\boldsymbol{H}\boldsymbol{H}^{\mathrm{T}}\boldsymbol{X}(N)\right]^{-1}\boldsymbol{X}^{\mathrm{T}}(N)\boldsymbol{H}\boldsymbol{H}^{\mathrm{T}}\boldsymbol{D}(N). \tag{16}$$

The Mathematical expectation can be obtained:

$$E(\hat{\boldsymbol{\theta}})=\boldsymbol{\theta}+\left[\boldsymbol{X}^{\mathrm{T}}(N)\boldsymbol{H}\boldsymbol{H}^{\mathrm{T}}\boldsymbol{X}(N)\right]^{-1}E\left[\left(\boldsymbol{H}^{\mathrm{T}}\boldsymbol{X}(N)\right)^{\mathrm{T}}\left(\boldsymbol{H}^{\mathrm{T}}\boldsymbol{D}(N)\right)\right]. \tag{17}$$

If the samples are infinite, the unbiased estimation can be obtained under the condition that the instrumental variable $\boldsymbol{H}$ is found by Eq. (18):

$$\begin{cases}\boldsymbol{H}^{\mathrm{T}}\boldsymbol{X}(N)\ \text{nonsingular}\\ \boldsymbol{H}^{\mathrm{T}}\boldsymbol{D}(N)=\boldsymbol{0}\end{cases} \tag{18}$$

As each matrix is not necessarily a square matrix, there will be irreversible problem. It is better to understand it in perspective of vector. Its mathematical essence is the construction of $\boldsymbol{H}$ to fulfill $\boldsymbol{H}^{\mathrm{T}}\boldsymbol{Y}(N)=\boldsymbol{H}^{\mathrm{T}}\boldsymbol{X}(N)\boldsymbol{\theta}$ such that the vector $\boldsymbol{H}^{\mathrm{T}}$ is strongly correlated with the vector $\boldsymbol{X}(N)$.

Therefore, this paper proposes a cyclic method to construct instrumental variables, the steps are as follows:

(1) $\hat{\boldsymbol{\theta}}=\left[\boldsymbol{X}(N)^{\mathrm{T}}\boldsymbol{X}(N)\right]^{-1}\boldsymbol{X}(N)^{\mathrm{T}}\boldsymbol{Y}(N)$;

(2) $\hat{\boldsymbol{Y}}(N)=\boldsymbol{X}(N)\hat{\boldsymbol{\theta}}$;

(3) By linear estimation $\boldsymbol{X}(N)$ in $\hat{\boldsymbol{Y}}(N)-\boldsymbol{X}(N)\hat{\boldsymbol{\theta}}=\boldsymbol{0}$, the intersection of the two solution spaces is obtained and then instrumental variables are found.

Obviously, the instrumental variables at this time meet the above conditions.

3 Structure and control system of 'Pioneer I'

Case selection and data acquisition are a crucial step to implement the algorithm. The deep-sea mining vehicle 'Pioneer I' (see Fig. 1), independently developed by Shanghai Jiaotong University, is taken as the research object in this paper.

From July 25th to August 3rd, 2021, the mining vehicle 'Pioneer I' successfully finished the 1305 m deep-sea trial in the South China Sea. It is 5.6 m long, 2.5 m wide, 2.0 m high and 9.0 t of air weight. It has the capability of seabed environment perception, intelligent control and efficient hydraulic mining.

The trials were carried out on seabed at 108 m, 246 m, 968 m and 1305 m below the sea level, respectively, consisting of launch and recovery, seabed path planning and autonomous walking and mining, providing sufficient information for system identification research.

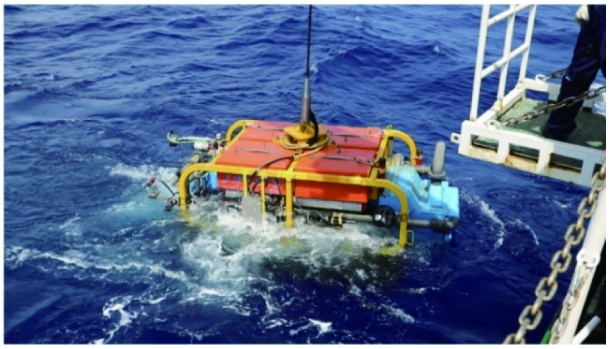

Fig. 1. Launch Process of 'Pioneer I'.

The overall equipment is made up of the power supply system, the administration center, the photoelectric transmission module, the motion management center, the hydraulic transmission system, the thrusters and the equipped sensors, as shown in Fig. 2, in which the administration center is accountable for path planning, mining instruction decision and status monitoring while the motion management center adopts PLC as the core to issue control instructions to the hydraulic system.

'Pioneer I' is a dual-track vehicle, and is driven by control

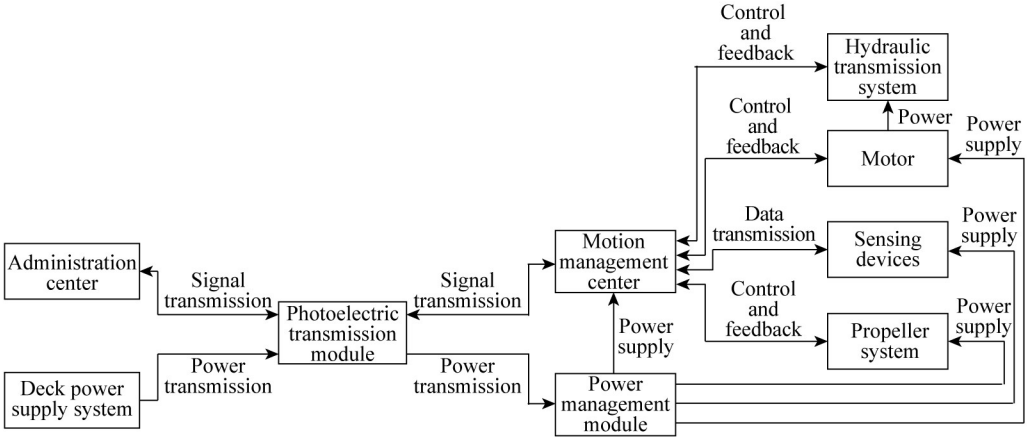

Fig. 2. Overall structure of 'Pioneer I'.

system. The hydraulic system is composed of controller, electro-hydraulic proportional valve, variable hydraulic pump, hydraulic motor and integrated navigation, which is shown in Fig. 3. The electro-hydraulic proportional valve changes the hydraulic oil flow and direction, so as to adjust the speed and steering of the motor, thus realizing forward, backward and turning actions. The integrated navigation module obtains the speed information as the feedback. From this perspective, it makes sense to identify the system as a transfer function to reflect its kinematic characteristics.

During the mining operation, however, the influence of environment is not static, accordingly the kinematic performance is time-varying: Due to the water hydraulic, the mechanical structure, especially the rack, would deform. The soil and obstacles would additionally affect the motion of the crawler, and the friction is time-varying. The motion command is also varying in different situations. The tension of the umbilical rope connecting the vehicle are not steady due to the uneven flow. The system time interval is not fixed. The refresh frequency is high, and the dimension of data matrix is high. The signal-to-noise ratio is high via fiber-optic umbilical cable communication, but the colored noise is not excluded. Therefore, the static mechanism modeling cannot reflect the real time state, and the modeling combined with experimental data can more truly reflect the actual state.

How to design an appropriate trial scheme for modeling has become the first point to be considered. Taking safety as core concern in practical operation, the power constraints, turning constraints, connection security of photoelectric composite cable must be taken into account, and thus, the ideal identification input conditions such as sweep frequency technique are not feasible. The real curvature motion data (position, velocity, angle, and the opening of the hydraulic valves on both sides of the tracks) are used as the identification statistic source to identify the model in recursive least square method and instrumental variable method.

4 System identification and parameter self-tuning controller

In this paper, the IV-RLS algorithm is used to model 'Pioneer I'. Firstly, the sea trial records are sorted and preprocessed, then data in different depth are used to establish the identification model and to exam the accuracy and generalization ability. Finally, based on the system identification model, the parameter self-tuning controller is designed and the control performance is analyzed, which displays the optimization impact of the simulation model.

4.1 Data preprocessing

In this sea trial, the intelligent walking test of 'Pioneer I' in different depth seabed was carried out, and the 'SJ' path was walked out (see Fig. 4). Since the main concern is to validate the maneuvering performance, the predetermined path is variable, including forward, backward and tuning motion in unknown environment, which requires precise control on the vehicles. The walking path measured by super-short baseline is as follows.

It takes up more than 10 minutes to finish this sea trial, recording 1597 sets of real-time monitoring data. Owing to long-distance signal transmission and communication characteristics of components, the refresh time interval varies from 0.1 to 1 s.

Firstly, the data is processed into equal time interval data, and the minimum time interval is used as the sampling time in system identification. Since the refresh frequency of various sensors is much higher than communication frequency, it applies to Shannon sampling theorem. For example, the refresh frequency of inertial navigation system is 50 Hz, so there is a phenomenon of repeated sampling, and the linear interpolation will not affect the accuracy of the model. Eq. (19) is used for interpolation:

$$u(k)=\frac{k-k_1}{k_0-k_1}u_0+\frac{k-k_0}{k_1-k_0}u_1, \tag{19}$$

where, u is the function of k, and the values at two points k_0 and k_1 are independent variables of u_0 and u_1, respectively; $u(k)$ is corresponding to k between the two points.

4.2 Model establishment and verification

As for the identification, the input and output data in pairs are processed to get the kinematic characteristics, and then it follows the fitting accuracy analysis by comparing the output distinction between simulation and the real data under the same input.

The IV-RLS estimation algorithm introduced in the third section is adopted, and the relevant calculation is done on the MATLAB platform. Then the fitting accuracy is calculated in X-Y-θ (turning angle) three channels and the 'SJ' trajectory is compared. Meanwhile, assessment indicators

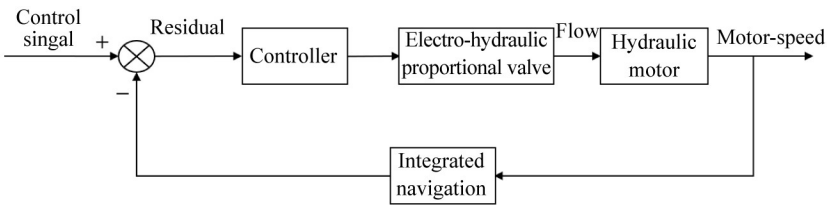

Fig. 3. Control system of 'Pioneer I'.

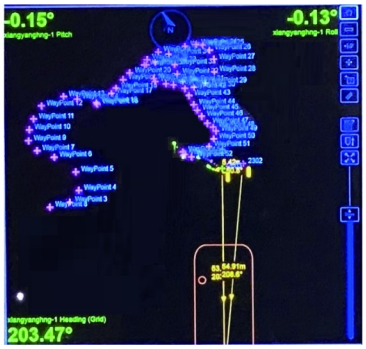

Fig. 4. Walking path 'SJ' measured by super-short baseline at 1305 m depth.

MMRE, VAF and R^2 are calculated for quantitative analysis. Then another identification algorithm based on neural network is adopted for algorithm comparison. Finally, another sea trial data is substituted into the model to confirm its generalization ability.

4.2.1 *Three-channel model and qualitative analysis*

It should be noted that the parameter identification of transfer function requires the information about the number of zeros and poles in advance. Here is a comprehensive consideration on system analysis to find the highest fitting accuracy of the zero-pole model.

The three-channel transfer function based on IV-RLS is as follows:

$$\frac{X_o(s)}{X_i(s)} = \frac{6.313\times10^5 s^3 + 8.04\times10^4 s^2 + 2029s + 136.5}{s^4 + 3.156\times10^6 s^3 + 8.529\times10^4 s^2 + 5274s + 141.1};$$

$$\frac{Y_o(s)}{Y_i(s)} = \frac{0.0741s^2 + 0.01666s + 0.004398}{s^3 + 0.3625s^2 + 0.04825s + 0.004482};$$

$$\frac{\theta_o(s)}{\theta_i(s)} = \frac{1048s^2 + 6.755s + 37.86}{s^3 + 1060s^2 + 6.204s + 38.09}, \tag{20}$$

where X_o, Y_o and θ_o are the output data and the others are the input data in three channels respectively.

Then real data and simulation response curve are plotted in Fig. 5 and Fig. 6 to verify the accuracy of the model.

4.2.2 *Evaluation indicators and quantitative analysis*

The average amplitude of relative error (*MMRE*), the ratio of variance (*VAF*) and coefficient of determination (R^2) have been used to affirm the fitting accuracy. Among them, *MMRE* represents the average value of regression error. The closer the value is to zero, the higher the fitting accuracy is. *VAF* is to measure the closeness between the actual data and the regression data in the form of percentage. A closer value to one indicates a higher fitting accuracy of the model. R^2 depicts the correlation between independent variables and dependent variables, which describes the change caused by independent variables accounts for the percentage of the total change. The value is between 0 and 1, and the closer it

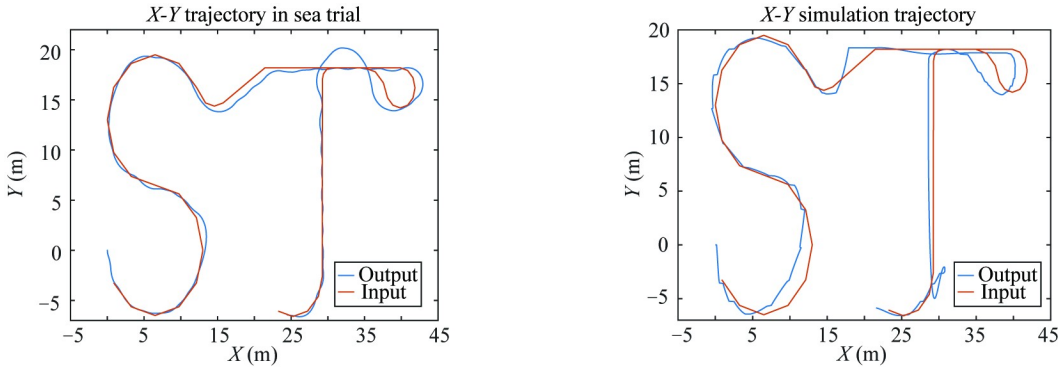

Fig. 5. Real trajectory and simulation trajectory.

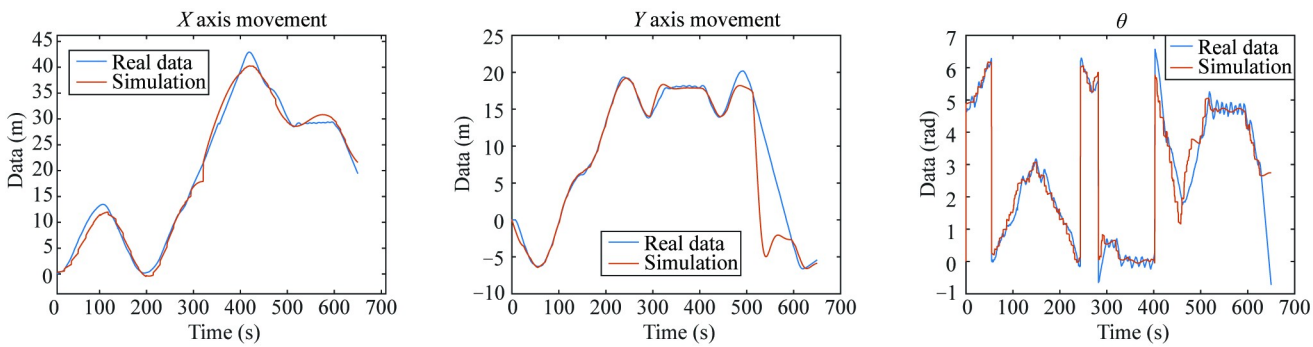

Fig. 6. *X-Y-θ* comparison between real and simulation trajectory at 246 m depth.

is to 1, the higher the correlation will be.

$$MMRE(r)=\frac{\sum_{i=1}^{N}\frac{\hat{r}(i)-r(i)}{r(i)}}{N}; \tag{21}$$

$$VAF(r,\hat{r})=\left\{1-\frac{var[r(i)-\hat{r}(i)]}{var[r(i)]}\right\}\times 100\%; \tag{22}$$

$$R-S_{\text{quared}}(r)=1-\frac{\sum_{i=1}^{N}[r(i)-\hat{r}(i)]}{\sum_{i=1}^{N}[r(i)-\bar{r}(i)]}. \tag{23}$$

It can be viewed from both diagrams above and numerical results in Table 1 that the accuracy of system identification model is satisfactory.

Table 1 Accuracy indicators in *X*, *Y* and θ channel

	MMRE	*VAF* (%)	R^2
X channel	0.1831	99.42	0.9929
Y channel	0.1850	95.61	0.9543
θ channel	0.5109	90.93	0.9092

For the fitting error, on the one hand, there are acquisition noise, observation error and model error. On the other hand, the characteristics of the control system should also be considered. The system response is divided into transient response and steady-state response. For the steady-state response, the steady-state error needs to be concerned. However, for the transient error, more attention is paid to the overshoot and response time. In other words, there are slight differences in the instantaneous transient error, such as different peak time and rise time.

4.2.3 *Algorithm comparison*

BP neural network (Error Back Propagation Neural Network) is adopted to process the data and here is the distinct performance. For the network setting, a two-layer feedforward network with sigmoid hidden neurons and linear output neurons is adopted to fit the three-dimension mapping. The network is trained with Levenberg-Marquardt backpropagation algorithm, and the number of hidden neurons is set to three as the optimum result. The order of the system is the same as that in Section 4.2.1.

Then real data and simulation response curve are plotted in Fig. 7 to show the performance of the algorithm.

It exhibits passable accuracy on the trajectory in *X*-*Y* dimension but series of peaks stand for imprecise high frequency characteristics, which manifests excessive sensitivity of noise.

For quantitative analysis, taking *X* channel as comparison, *MMRE* is 0.204, and *VAF* is 0.9954, R^2 is 0.995. Combined with trajectory, it shows an overfitting model. However, the parameters really affect the model accuracy of BP neuron network, which ought to be a future work to explore.

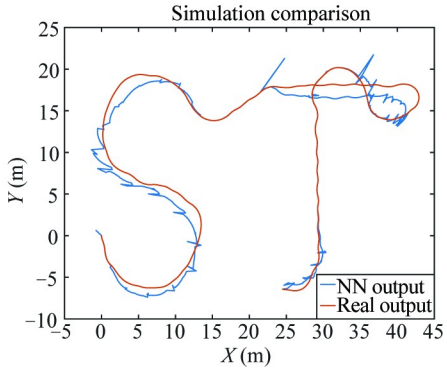

Fig. 7. *X*-axis comparison between real and simulation trajectory at 1305 m depth.

4.2.4 *Generalization ability analysis*

Finally, another sea trial data is substituted into the model to verify its generalization, as shown in Fig. 8.

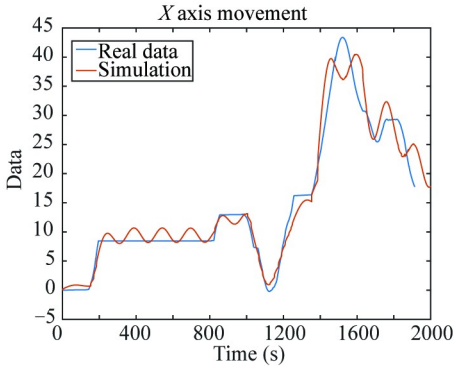

Fig. 8. *X*-axis comparison between real and simulation trajectory at 1305 m depth.

Similarly, the *X*-axis data is analyzed, $MMRE = 0.3186$, $VAF = 95.32\%$, $R^2 = 0.9519$.

The model can also reflect the kinematic characteristics even at different depths. From the statistical characteristics, the results show accuracy and stronger generalization.

4.3 Parameter self-tuning controller

The next point is to improve the kinematic performance based on the model. The kinematic performance is closely related to servo control parameters. It generally takes an amount of time to design and test the structure and parameters of controller to obtain stable, accurate and fast response. Combined with the simulation model of the system identification, the frequency domain analysis method can complete the parameter design, for which the toolbox MATLAB PID Tuner provides a concise platform.

The input and output record data on *X* channel are analyzed in Fig. 9 (the other two channels are similar). It can be seen that at about 320 s, there is a long response time and overshoot in the original system, but steady-state error in

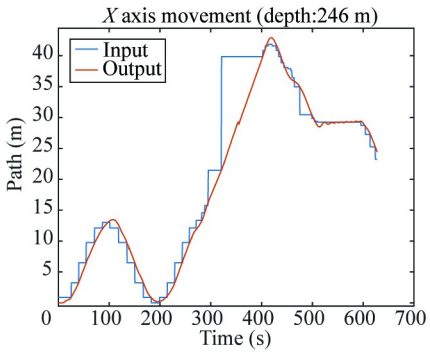

Fig. 9. Input and output record data on *X* channel.

each step is close to 0. The simulation system in Fig. 10 shows the same performance. The optimal performance is shown in Fig. 11.

Intuitively, it is obvious that the control performance in Fig. 11 is greatly improved by parameter self-tuning controller. The maximum response time of each step command is less than 2 s, and the overshoot is almost zero. The oscillation disappears, and the steady-state error is close to 0.

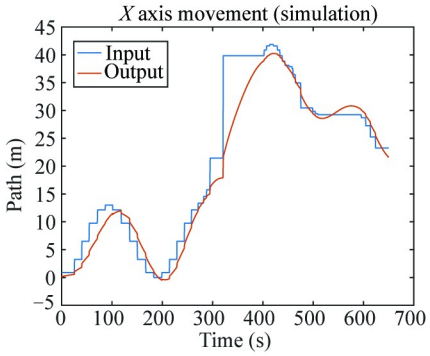

Fig. 10. Input and output simulation data on *X* channel.

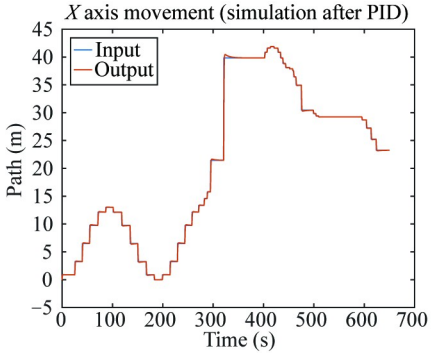

Fig. 11. Input and output data on *X* channel after self-tuning controller.

5 Conclusions

In this paper, a digital prototype with generalization ability and practical applicability for deep-sea mining vehicles has been built. Combined with the system design of 'Pioneer I' and real sea trial data, a system identification algorithm IV-RLS has been conceived to obtain the kinematic model which fitting accurately into *MMRE*, *VAF* and R^2 respectively. Data experiments under multiple conditions show that the model has good generalization ability, which is suitable for mining vehicle operation in various water depths and sea conditions.

Combined with time-frequency domain analysis, the parameter self-tuning controller has been designed for the model. Numerical experiments show that the control performance has been essentially improved: shorter response time and diminished tracking error, reflecting the great significance of system identification for the design and test.

In future work, system identification can contribute to the life cycle health management, realizing the full monitoring of the system, shedding light to deep-sea operation.

References

Bai, W.W., Ren, J.S. and Li, T.S., 2018. Multi-innovation gradient iterative locally weighted learning identification for a nonlinear ship maneuvering system, *China Ocean Engineering*, 32(3), 288–300.

Chen, F., Ganier, H. and Gilson, M., 2013. Refined instrumental variable identification of continuous-time OE and BJ models from irregularly sampled data, *IFAC Proceedings Volumes*, 46(11), 80–85.

Chen, Z.J., 2009. Optimization of neural network based on improved genetic algorithm, *2009 International Conference on Computational Intelligence and Software Engineering*, IEEE, Wuhan, China.

Deng, K.P. and Ding, F., 2014. Newton iterative identification method for an input nonlinear finite impulse response system with moving average noise using the key variables separation technique, *Nonlinear Dynamics*, 76(2), 1195–1202.

Deng, P., Zeng, L.C. and Liu, Y., 2018. RBF neural network backstepping sliding mode adaptive control for dynamic pressure cylinder electrohydraulic servo pressure system, *Complexity*, 2018, 4159639.

Gao, N.X., 2006. *Design of Driving System and Controller of Lunar Rover*, MSc. Thesis, Jilin University, Jilin. (in Chinese)

Guan, X.P. and Chen, C.L., 2004. Delay-dependent guaranteed cost control for T-S fuzzy systems with time delays, *IEEE Transactions on Fuzzy Systems*, 12(2), 236–249.

Guo, F., Wu, O.Y., Ding, Y.S. and Huang, B., 2017. A data-based augmented model identification method for linear errors-in-variables systems based on EM algorithm, *IEEE Transactions on Industrial Electronics*, 64(11), 8657–8665.

Huang, R.M. and Li, X.S., 2019. Design and test of speed control and trajectory tracking for deep-sea mining vehicle, *Mining and Metallurgical Engineering*, 39(3), 20–24. (in Chinese)

Ji, H.T., Fan, J. and Huang, X.L., 2008. Experimental study and system identification of hydrodynamic force acting on heave damping plate, *China Ocean Engineering*, 22(1), 141–149.

Jia, H.L., Wang, Z.J., Cao, M.S. and Li, J., 2020. Damage identification in cantilever beams based on high-order frequency response function with improved sensitivity, *Journal of Testing and Evaluation*, 48(5), 20180712.

Kong, S., Cui, H.Y., Wu, G. and Ji, S.Y., 2020. Full-scale identification of ice load on ship hull by least square support vector machine method, *Applied Ocean Research*, 106, 102439.

Li, D.D., Lin, Y. and Zhang, Y., 2018. A track initiation method for the underwater target tracking environment, *China Ocean Engineering*, 32(2), 206–215.

Li, D.G. and Shu, Y.Q., 2009. Research of parameter identification

algorithm of intake port fuel film model for gasoline engine, *Transactions of CSICE*, 27(4), 363–369. (in Chinese)

Wada, R., Waseda, T. and Jonathan, P., 2016. Extreme value estimation using the likelihood-weighted method, *Ocean Engineering*, 124, 241–251.

Wang, Z.H., Xu, H.T., Xia, L., Zou, Z.J. and Soares, C.G., 2020. Kernel-based support vector regression for nonparametric modeling of ship maneuvering motion, *Ocean Engineering*, 216, 107994.

Watanabe, K., Murakami, H., Kitano, M. and Katahira, T., 1993. Experimental characterization of dynamic soil-track interaction on dry sand, *Journal of Terramechanics*, 30(2), 111–131.

Yazid, E. and Ng, C.Y., 2021. Identification of time-varying linear and nonlinear impulse response functions using parametric Volterra model from model test data with application to a moored floating structure, *Ocean Engineering*, 219, 108370.

Zamani, A.R. and Badri, M.A., 2015. Wave energy estimation by using a statistical analysis and wave buoy data near the southern Caspian Sea, *China Ocean Engineering*, 29(2), 275–286.

Zhang, Y.N., Li, W., Yi, C.F. and Chen, K., 2008. A weights-directly-determined simple neural network for nonlinear system identification, *2008 IEEE International Conference on Fuzzy Systems*, IEEE, Hong Kong, China.

Zhou, L., Li, L. and Li, X.F., 2009. Design and optimization of a multi-degree-of-freedom articulated mechanism, *Modern Manufacturing Engineering*, (9), 120–123, 111. (in Chinese)

Zhou, Z.J., Yang, N. and Wang, Z., 2013. Analysis on shock wave speed of water hammer of lifting pipes for deep-sea mining, *China Ocean Engineering*, 27(2), 205–214.